J. Fluid Mech. (1983), *vol.* 126, *pp.* 219–235
Printed in Great Britain

Resonance in open harbours

By CLAUDE F. NOISEUX
Division of Applied Sciences, Harvard University, Aiken Computation Laboratory, Cambridge, Massachusetts 02138

(Received 26 May 1981 and in revised form 2 July 1982)

The effect of depth variations near the mouth of harbour-like geometries is investigated. It is found that some modes of oscillation that, for uniform depth, would decay rapidly can be trapped very effectively when moderate increases in depth occur at the seaward end of the harbour.

1. Introduction

Analytical studies of small-amplitude water waves have shown that there are conditions that can lead to resonant or trapped waves in coastal regions. There are roughly two types of model geometries in which resonant behaviour has been shown to exist. The first group consists of harbours that are connected to the outlying ocean via a narrow channel or constriction. The frequencies at which long-term ringing can occur in such a geometry are then closely related to the natural frequencies associated with the shape of the virtually finite interior domain. A constant-depth hypothesis is characteristic of these studies (Ippen 1966; Krautchenko & McNown 1955; Lee 1971).

More recently, wave trapping has also been shown to occur in unbounded domains. Coastline regions with an appropriate offshore depth variation can support waves whose structure confines the bulk of the energy to the immediate vicinity of the shore, resulting in certain types of persistent waveforms. Owing to the analytical difficulties, variable-depth models are typically studied in either one space dimension (Kajiura 1961; Roseau 1952) or in geometries where the governing equations are separable (Lautenbacher 1970; Shen, Meyer & Keller 1968).

In this study, some of the consequences of variable width and changing depth are explored via the linear shallow-water equations in geometries resembling an open (unconstricted) bay such as that of figure 1. The e-folding time of oscillations that are initially localized in such a 'harbour' would be very small if the depth of the cavity were the same as that in the reservoir. It can be shown, however, that there are many idealized planform geometries for which the inclusion of significant deepening in the seaward direction results in no radiation losses from the cavity. Thus it seems highly plausible that, for some real open-bay geometries, the observed slow decay rates of selected modes are due to this implication of the geometry. One possible example of the phenomenon would be the long-term ringing of particular modes in some harbours after inundation by a tsunami.

In this paper, the shallow-water problem is formulated for a family of geometries, each of which is a simplified counterpart of that in figure 1. Initially, the objective is to calculate the transmission properties for wave radiation from the cavity into the reservoir. Subsequently, these results are used to determine the complex natural frequency of the system in the mode of interest.

It is not the objective of this study to provide detailed information concerning the oscillations in any particular real harbour, nor is there any intent to address the excitation by external sources of such modes of oscillation.† Rather, the aim is to characterize clearly the conditions under which effective trapping can occur and to provide a quantitative account of the parameter dependence of the decay time.

2. Field equations and idealized geometries

The appropriate differential equation for the study, in the linear regime, of waves whose horizontal scale is large compared with depth, is the linear shallow-water equation (Stoker 1957)

$$\tilde{h}(\tilde{x},\tilde{y})\,\nabla^2\Phi + \nabla\tilde{h}\,.\,\nabla\Phi = \frac{1}{g}\,\Phi_{tt} \tag{2.1}$$

for the velocity potential $\Phi(\tilde{x},\tilde{y},t)$. This equation governs the dynamics of the fluid bounded by an underlying depth distribution $\tilde{h}(\tilde{x},\tilde{y})$, and by vertical sidewalls, on which the boundary condition $\partial\Phi/\partial n = 0$ is imposed. The theory is well-suited for this analysis owing to its relative simplicity and, given typical harbour parameter values, its ability to yield accurate answers. A harbour profile representative of those to be considered is shown in figure 1.

The bay geometries are taken to be highly idealized rectangular gulfs, with the back end of the harbour at $\tilde{x} = -\tilde{L}$, opening out into the deep ocean as $\tilde{x}$ becomes positive. To the left of $\tilde{x} = 0$, the profile tends to a constant depth h_0 and a width $2b\pi$. For simplicity the variety of profiles is further limited to those shapes where $\tilde{L}/2b\pi$ is substantially greater than 1. In principle, no such limitation is necessary, but the calculation for shorter geometries would be more difficult and would add little insight into the phenomenon.

In such geometries, it can be expected that after some initial excitation (e.g. a tsunami) the behaviour near $\tilde{x} = -\tilde{L}$ will eventually settle into some combination of the parallel-plate waveguide modes. To examine the possibility of trapping some of these modes in the harbour's interior, it is useful to consider first the steady-state wave problem associated with the infinite geometry suggested by the dotted lines in figure 1. The question may then be phrased – what is the reflection coefficient associated with waves incident from the left on the transition region, and, in particular, under what conditions will these waves undergo such strong reflections that, owing to the variable geometry in $\tilde{x} \lesssim 0$, they are virtually (or completely) confined to the interior of the harbour? The central task of this study is to find the reflection coefficient as a function of the geometry-characterizing parameters, but, in §5 the answers derived for the idealized shapes will be used to determine the amplitude decay rate in a harbour of finite extent.

Equation (2.1) is cast in dimensionless form through the introduction of a normalized depth function h and new coordinates u, v, where

$$\tilde{x} = ub, \quad \tilde{y} = vb, \quad \tilde{h} = h_0 h(x,y).$$

Then, for 'steady-state' waves

$$\Phi(\tilde{x},\tilde{y},t) = e^{-i\omega t}\phi(u,v)$$

† For the tsunami excitation, for example, the deposition of energy is associated with a highly nonlinear inundation process.

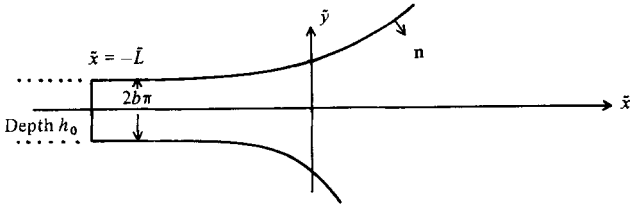

FIGURE 1. Idealized geometry.

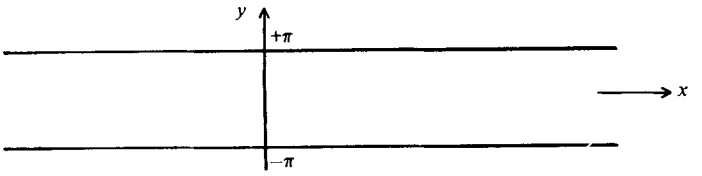

FIGURE 2

the governing equation becomes

$$h(u,v)\nabla^2\phi + \nabla h \,.\, \nabla\phi + K_0^2\phi = 0, \tag{2.2}$$

where a dimensionless wavenumber $K_0^2 = \omega b/(gh_0)^{\frac{1}{2}}$ has been introduced.

In §3, a family of conformal-mapping functions is adopted that relates a set of interesting geometries in the physical (u,v)-plane, to a single, simpler geometry in the mapped domain. The competing effects of depth and width variation will then be explicit in the new equation for ϕ.

3. Conformal mapping of the shallow-water equation

The region in the (u,v)-plane is mapped onto an infinite strip of width 2π in the (x,y)-plane (figure 2). The physical and mapped domains are related by an analytic function f of the complex variable z:

$$w = u + iv = f(z) = f(x+iy).$$

For such a function, the following statements are true:

$$\text{(i)} \quad \frac{\partial^2\phi}{\partial u^2} + \frac{\partial^2\phi}{\partial v^2} = |f'(z)|^{-2}\left(\frac{\partial^2\phi}{\partial x^2} + \frac{\partial^2\phi}{\partial y^2}\right),$$

$$\text{(ii)} \quad h_u\phi_u + h_v\phi_v = |f'(z)|^{-2}(h_x\phi_x + h_y\phi_y),$$

$$\text{(iii)} \quad \frac{\partial\phi}{\partial n(u,v)} = 0 \quad \Rightarrow \quad \frac{\partial\phi}{\partial n(x,y)} = 0.$$

The boundary-value problem in the mapped plane,

$$h\nabla^2\phi + \nabla h \,.\, \nabla\phi + K_0^2|f'(z)|^2\phi = 0, \tag{3.1a}$$

with

$$\frac{\partial\phi}{\partial y} = 0 \quad (y = \pm\pi), \tag{3.1b}$$

now exhibits an effective wavenumber $K_0^2|f'(z)|^2$ that is the function of position. This is characteristic of an inhomogeneous medium and it depends only on the width variations.

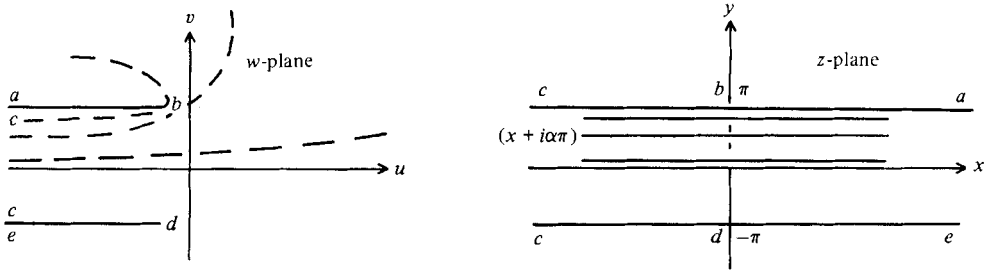

FIGURE 3

A mapping function with sufficient flexibility to be a suitable approximation to the most macroscopic features of the interesting geometries is developed in stages. Consider first the function f with derivative

$$f' = 1 + e^z. \tag{3.2}$$

The strip in the z-plane maps to the entire w-plane exterior to the two cuts emanating from $(-1, \pi)$ and $(-1, -\pi)$ (figure 3). The dotted lines in the w-plane are the images of the three lines $z = x + i\alpha\pi$. For different values of α $(0 < \alpha \leqslant 1)$ the parallel lines $z = x + i\alpha\pi$ correspond to the streamlines (a curve along which $\partial\phi/\partial n = 0$) of the potential-flow problem associated with the semi-infinite plate geometry in the w-plane. Alternatively, the z-variable can be scaled by α, defining a new mapping

$$w' = 1 + e^{\alpha z}, \tag{3.3}$$

or, upon integration,

$$\alpha w = \alpha z + e^{\alpha z}. \tag{3.4}$$

The images of the lines $z = x \pm i\pi$, for different values of α, generate streamlines symmetric about the u-axis, but uniformly magnified in u and v by a factor $1/\alpha$; a consequence made evident by (3.4). The latter function is preferable to (3.2) since the spacing of the boundaries at $u = -\infty$ in the w-plane is the same for all values of α. The parameter α determines the 'flare angle' of the cavity. As $\alpha \to 1$, the profile opens most rapidly, and as $\alpha \to 0$ the harbour opens very gradually. In this case, however, the region where the channel's widening is most pronounced tends to $+\infty$ since it is scaled by $1/\alpha$. A second parameter β is introduced to circumvent this difficulty. With $\alpha = 1$ and $\beta \neq 1$, the mapping

$$w' = f'(z) = (1 + e^{\alpha z})^{\beta} \tag{3.5}$$

takes the infinite strip in the z-plane to a horn-shaped region (figure 4). The horn opens to include a small flare angle $2\pi\beta$ when β is small. With α less than 1 the corners are rounded out and the dotted lines show the images of $z = x \pm i\pi$, which form a net flare angle of $2\pi\alpha\beta$. This method of creating slowly varying profiles localizes the onset of opening to the neighbourhood of the origin. The parameter β is also used to prescribe the curvature of the boundary near $u = v = 0$. Thus a variety of shapes can be studied which all have the same net flare at $+\infty$. The extent to which the reflection process is governed by the local geometry can then be evaluated.

A third parameter δ $(0 < \delta \leqslant 1)$ is introduced to generate shapes that are not symmetric about the u-axis. As an extended form of (3.3), the mapping $f(z)$ with derivative

$$f'(z) = 1 + e^{iy_0} e^{\frac{1}{2}(\alpha+\delta)z} \quad (y_0 = \tfrac{1}{2}\pi(\alpha - \delta), \tag{3.6}$$

takes the lines $z = x + i\pi$ and $z = x - i\pi$ into curves in the (u, v)-plane whose final

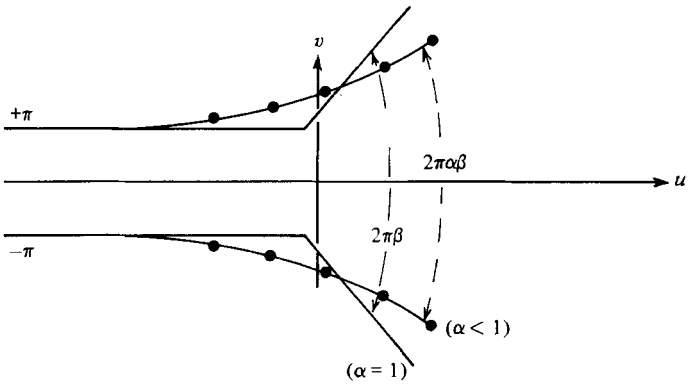

FIGURE 4

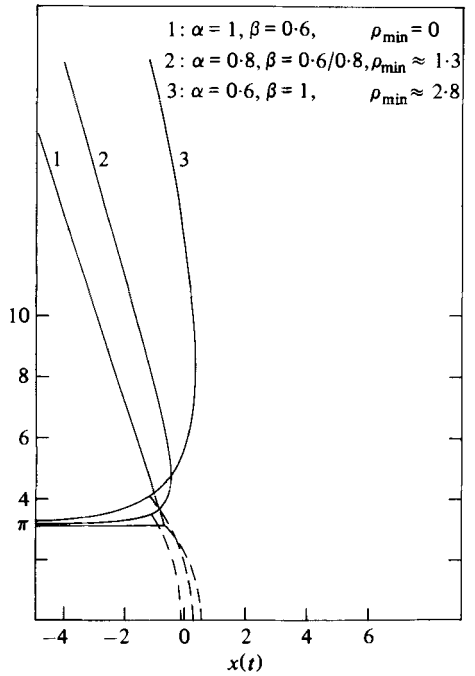

FIGURE 5

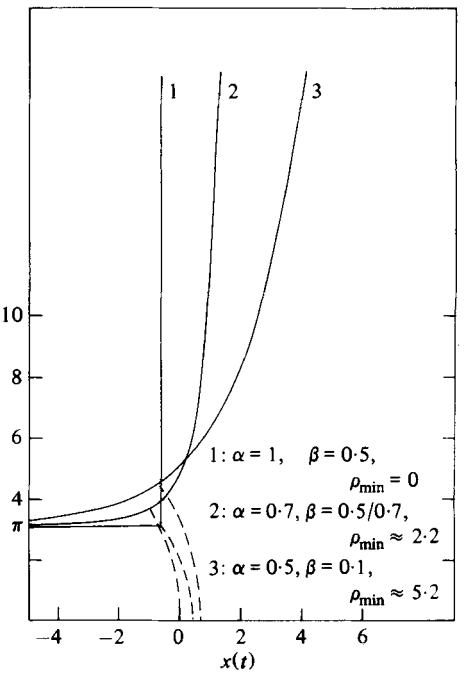

FIGURE 6

FIGURE 5. Symmetric harbour shapes with opening angle $0{\cdot}6 \times 2\pi$.

FIGURE 6. Symmetric harbour shapes with opening angle $0{\cdot}5 \times 2\pi$.

angles with respect to the u-axis are $\alpha\pi$ and $-\delta\pi$ respectively. The spacing of the boundaries at $u = -\infty$ in the w-plane is again the same (2π) for all values of α and δ, and the net included angle at $u = +\infty$ is now $(\alpha+\delta)\pi$. Furthermore, the function $f'(z)$ as given by (3.6) can again be raised to the power β to control the local curvature near the origin. Various shapes generated by the final mapping function f, with derivative

$$f'(z) = (1 + e^{iy_0} e^{\frac{1}{2}(\alpha+\delta)z})^{\beta}, \tag{3.7}$$

are shown in figures 5–7. An alternative description of the harbour shapes generated by (3.7) can also be used. Specifying the net opening angle $2\pi\gamma$ ($= (\alpha+\delta)\,\pi\beta$) and the minimum radii of curvature ρ_+, ρ_- of the top and bottom branches of the profile is equivalent to specifying α, δ, β in (3.7) (see the appendix), and usefully separates

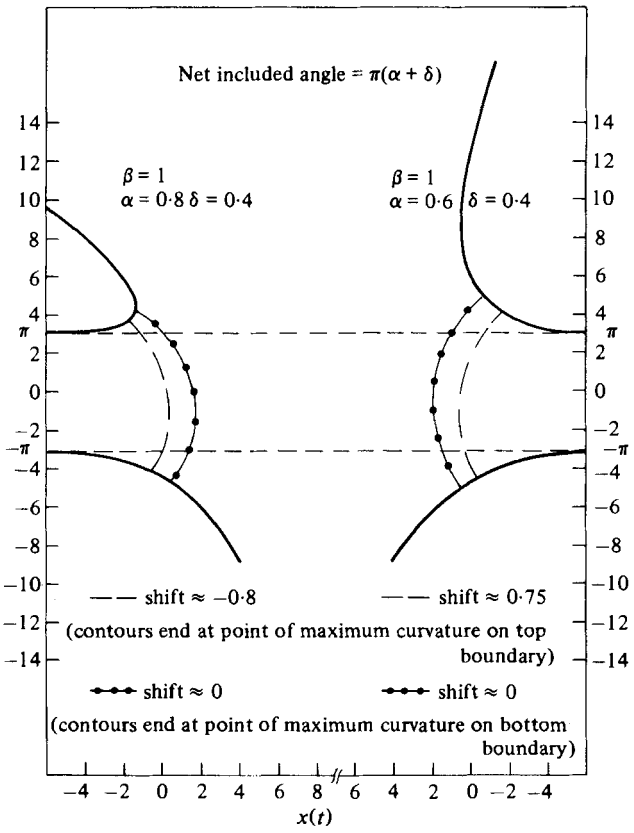

FIGURE 7. Asymmetric harbour shapes.

the local and far-field descriptions of a given shape. Figures 5 and 6 show the upper halves of symmetric bays ($\alpha = \delta$, $\rho_+, \rho_- \equiv \rho_{\min}$) that open to include angles of $0{\cdot}6 \times 2\pi$ and $0{\cdot}5 \times 2\pi$, respectively. Two additional examples with $\gamma = 0{\cdot}6$ and $0{\cdot}5$ are given in figure 7 which are asymmetric about $u = 0$. For each harbour shape in the three figures, a dashed line is drawn representing the image of a line $x =$ constant in the mapped plane, which terminates at the point of minimum radius of curvature of the boundary.

The depth function is chosen to have simple behaviour in the mapped plane. Only functions $h(u, v)$ are considered that reduce to $h(x)$ when mapped. In the physical plane, constant-depth contours intersect the boundaries at right angles, and the dashed lines in figures 5–7 are examples of such contours. The function $h(x)$ to be used is

$$h(x) = \tfrac{1}{2}(1 + h_2) + \tfrac{1}{2}(h_2 - 1) \tanh \tfrac{1}{2}s(x + \text{SHIFT}), \tag{3.8}$$

where h_2 is the final depth at $x = \infty$, $2\pi/s$ is a rough measure of the depth transition length, and the position of the mean depth $\frac{1}{2}(1 + h_2)$ is located by specifying the value of SHIFT. When $-s(x + \text{SHIFT}) \gg 1$, $h(x)$ is equal to 1. As x increases, the depth increases monotonically and approaches its final value h_2 when $s(x + \text{SHIFT}) \gg 1$. The parameter s allows for local adjustment of the depth contours while retaining the same far-field values. Graphs of $h(x)$ for $h_2 = 2$ and various values of s, are given in figure 8.

With the mapping function $f(z)$ and depth $h(x)$ as specified, a parametric study may now be undertaken for solutions of (3.1). Each set of values (α, δ, β, s, h_2) in (3.1)

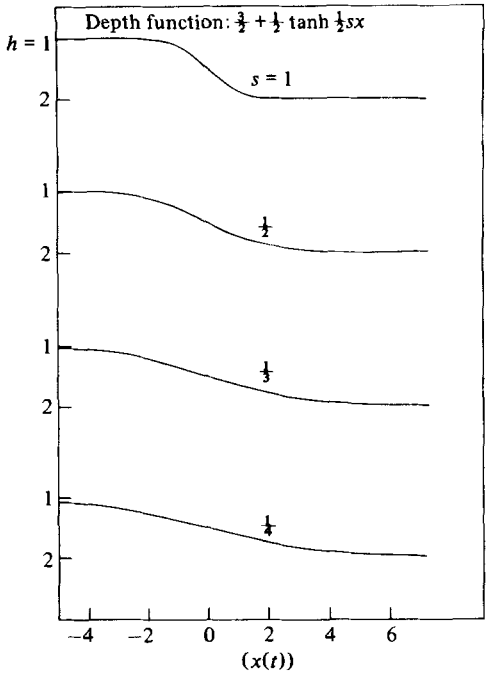

FIGURE 8. Depth functions.

corresponds to a different harbour in the physical (u, v)-plane. Before detailing the solution procedure, however, the origins of the resonance will be outlined by considering (3.1) directly.

The single derivative term in (3.1) is eliminated by defining ψ such that

$$\phi(x, y) = h^{-\frac{1}{2}}(x)\,\psi(x, y).$$

The resulting equation,
$$\nabla^2\psi + P(x, y)\,\psi = 0, \tag{3.9}$$

where
$$P(x, y) = \left[\frac{K_0^2}{h(x)}\,|f'(z)|^2 - \left(\frac{1}{4}\left(\frac{h_x}{h}\right)^2 + \frac{1}{2}\left(\frac{h_x}{h}\right)_x\right)\right], \tag{3.10}$$

exhibits the possibility that variable-depth contributions may, in some regions, be sufficient to produce a negative value for $P(x, y)$. More precisely, the rapid exponential growth associated with widening,

$$\frac{K_0^2}{h}\,|f'(x)|^2 = \frac{K_0^2}{h}\,(1 + 2e^{\frac{1}{2}(\alpha+\delta)x}\cos(y_0 + \tfrac{1}{2}(\alpha+\delta)y) + e^{(\alpha+\delta)x})^{\beta} \quad (y_0 = \tfrac{1}{2}\pi(\alpha-\delta)),$$

and the manner in which the slope h_x enters the expression

$$\frac{1}{4}\left(\frac{h_x}{h}\right)^2 + \frac{1}{2}\left(\frac{h_x}{h}\right)_x,$$

suggest that negative values of $P(x, y)$ occur near the origin. One possibility for $h(x)$, together with its consequences, is illustrated in figure 9. In both limits $x \to \pm\infty$,

$$P(x, y) = \frac{K_0^2}{h}\,|f'(z)|^2 > 0,$$

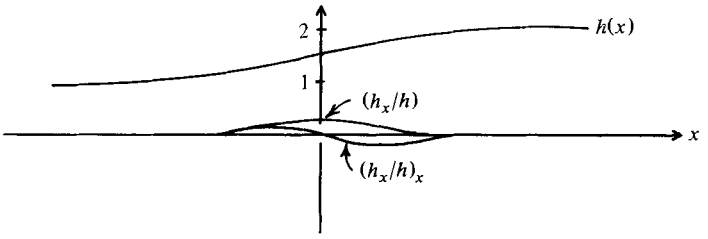

FIGURE 9

and wavelike solutions are expected. To the left of the origin, however, where

$$\frac{1}{4}\left(\frac{h_x}{h}\right)^2+\frac{1}{2}\left(\frac{h_x}{h}\right)_x > 0$$

and $|f'(z)|^2$ is moderate in size, proper adjustment of the parameters leads to a region in the strip where exponential (non-oscillatory) solutions prevail. There exist two 'turning lines' in the strip, and, as with turning points in ordinary differential equations, significant reflections occur as a wave encroaches upon this zone. It is emphasized that the existence of a region in the strip where $P(x, y) < 0$ depends only on the geometry of the harbour. In particular, the tunnelling zone is independent of the boundary conditions imposed at $x = \pm\infty$. Thus not only may waves originating in the harbour have trouble getting out, but it is also true that waves in the ocean propagating landwards may be reflected back out to sea, in such a way that they have little impact on the inner portions of the bay. Though the method of solution to be described in §4 would be entirely appropriate for this more complicated problem, its solution will not be considered here. For the purpose of characterizing the qualitative features of the resonance, only the computationally simpler case of modes leaking out of the harbour will be dealt with in this study. This leads to the simplest set of boundary conditions and addresses the issue of possible long-term ringing in a harbour after the arrival of a tsunami.

4. Eigenfunction representation

The regular geometry of the mapped plane suggests the representation

$$\psi(x, y) = \sum_{n=0}^{\infty} \psi_n(x) \cos \tfrac{1}{2}n(y-\pi),$$

which satisfies the boundary conditions $\partial\psi/\partial y = 0$ when $y = \pm\pi$. The variable coefficient term (in y) of (3.10) is expressed in the product-series form

$$|f'(z)|^2 = [1+2\exp(\tfrac{1}{2}(\alpha+\delta)x)\cos(\tfrac{1}{2}\pi(\alpha-\delta)+\tfrac{1}{2}(\alpha+\delta)y)+\exp(\alpha+\delta)x]^{\beta}$$

$$= 1+\sum_{m=0}^{\infty} a_m(x)\cos\tfrac{1}{2}m(y-\pi), \tag{4.1}$$

to ensure that $a_m(x) \to 0$ as $x \to -\infty$, for all m. Inserting the two series representations into (3.9) yields a coupled system of ordinary differential equations for the mode functions $\psi_n(x)$. The plane-wave mode ($n = 0$) is governed by

$$\psi_0''(x)+\left[\frac{K_0^2}{h}(1+a_0)-G\right]\psi_0+\frac{K_0^2}{h}\sum_{n=1}^{\infty}\tfrac{1}{2}a_n\psi_n = 0,$$

and for $n \geqslant 1$ the equations are

$$\psi_n''(x)+\left[\frac{K_0^2}{h}(1+a_0+\tfrac{1}{2}a_{2n})-G-\tfrac{1}{4}n^2\right]\psi_n+a_n\psi_0\frac{K_0^2}{h}$$
$$+\frac{K_0^2}{h}\sum_{l=1}^{\infty}{}^{(l\neq n)}\,\tfrac{1}{2}\psi_l(a_{l+n}+a_{|l-n|})=0, \quad (4.2)$$

where
$$G=\frac{1}{4}\left(\frac{h_x}{h}\right)^2+\frac{1}{2}\left(\frac{h_x}{h}\right)_x.$$

The behaviour of the nth mode is determined by

$$S_n(x)\equiv\frac{K_0^2}{h}(1+a_0(x)+\tfrac{1}{2}a_{2n}(x))-G-\tfrac{1}{4}n^2 \quad (4.3)$$

when coupling is negligible, where S_n represents the modal decomposition of (3.10). As $x\to-\infty$, where depth and width variations cease,

$$S_n\to K_0^2-\tfrac{1}{4}n^2\equiv K_n^2,$$

and wave motion only occurs if $K_n^2>0$. The long-wave (small-K_0) assumption inherent in this development implies that most modes will be evanescent when $x\ll 0$. In this region the system of equations simplifies to

$$\psi_n''+K_n^2\psi_n=0 \quad (n=0,1,2,\ldots). \quad (4.4)$$

The complete solution in this domain is a collection of parallel plate waveguide modes

$$e^{-i\omega t}\cos\tfrac{1}{2}n(y-\pi)\,[A_n e^{iK_n x}+B_n e^{-iK_n x}].$$

At a fixed value of x, this represents the 'sloshing mode' (or ringing) behaviour within the idealized harbour. Energy is released into the outlying ocean by the combination of terms $e^{-i\omega t}A_n e^{iK_n x}$. Reflected waves $e^{-i\omega t}B_n e^{-iK_n x}$ are present owing to the variable geometry. The complex constants $R_n=B_n/A_n$ are defined as the nth-mode reflection coefficients, and their size is a measure of the amount of wave blocking associated with that mode.

This study will be limited to the simplest, and, in view of the wave cutoff in K_n, most likely case of mode 1 ($\sim\sin\frac{1}{2}y$) ringing within the harbour. The boundary condition at $x=-\infty$ for this situation is given schematically as

$$\begin{matrix}\psi_0\\ \psi_1\\ \psi_2\\ \vdots\end{matrix}\quad\begin{Bmatrix}0 & R_0 e^{-iK_0 x}\\ 1\ e^{iK_1 x} & R_1 e^{-iK_1 x}\\ 0 & R_2 e^{-iK_2 x}\\ \vdots & \vdots\end{Bmatrix}. \quad (4.5)$$

The first column in the matrix consists of forward-moving waves where the first odd mode has unit amplitude while the remaining mode amplitudes are set equal to zero. The second column contains reflected waves with unknown complex amplitudes. Propagation in the ψ_1 mode requires that K_0 be greater than 0·5. As the modenumber increases, a value of n occurs for which $K_n^2=K_0^2-\frac{1}{4}n^2<0$, and the branch of the square root is chosen to secure decaying solutions in the negative domain. The further restriction $K_0<1$ will also be imposed. This merely ensures that only ψ_0 and ψ_1 are nonvanishing as $x\to-\infty$, thereby reducing the computational effort.

The boundary conditions on the ψ_n at $x=+\infty$ are chosen to correspond to outgoing waves in the physical (u,v)-plane. Owing to the unbounded behaviour of the Fourier coefficients $a_m(x)$ in (3.2) as $x\to\infty$, it proves advantageous to use a new

set (t, ϕ_n) of dependent and independent variables. Though the equations which result will not be recorded here, it is of some interest to note that the 'optimal' choice of variables is dictated by the mapping function f:

$$t = x + e^{\gamma x}, \quad \psi_n = (1 + e^{\gamma x})^{-\frac{1}{2}} \phi_n \quad (\gamma = \tfrac{1}{2}(\alpha + \delta)\beta), \tag{4.6}$$

where t represents a simplified form of $f(z)$ along the line of effective symmetry $y = y_0$ in the mapped plane. When (4.2) is recast in terms of t and ϕ_n, the system decouples to (4.4) as $t \to -\infty$ (since $t \to x$ and $\phi_n \to \psi_n$ in that limit) and also decouples to

$$\phi_n''(t) + \frac{K_0^2}{\gamma^2 h_2} \phi_n(t) = 0 \quad (n = 0, 1, 2, \ldots) \tag{4.7}$$

as $t \to +\infty$. In contrast with the negative $-t$ domain, all modes have oscillatory solutions as $t \to +\infty$, for all K_0, provided the final depth h_2 is finite. This insures that there will always be some energy leakage out of the harbour. From (4.7), incoming and outgoing waves may now be readily distinguished, and the radiation condition is enforced provided that each mode is forced to take the limiting form

$$\phi_n(t) \sim T_n \exp \frac{iK_0 t}{\gamma h_2^{\frac{1}{2}}} \quad (n = 0, 1, 2, \ldots) \tag{4.8}$$

as $t \to \infty$, where T_n are the unknown transmission coefficients. This completes the specification of the two-point boundary-value problem. Before presenting the numerical results, however, an important feature of the governing equations should be noted. Symmetry of the harbour profile ($\rho_+ = \rho_-$, or $\alpha = \delta$ in the mapping function) manifests itself in a significant simplification of the coupled system (4.2). The left-hand side of (4.1) remains unchanged when y is replaced by $-y$. This invariance extends to the right-hand side for all y provided that $a_{2m+1}(x) = 0$ $(m = 0, 1, 2, \ldots)$, implying an even/odd decoupling of the system. A wave propagating in the nth mode ϕ_n is only coupled to other modes ϕ_m when m has the same parity as n. Thus with the boundary conditions (4.5) and (4.8), no even-mode behaviour is initiated within the channel when $\alpha = \delta$. Some of the implications of this fact will be drawn in the next section.

The solution of the coupled system, for selected values of α, δ, β, s, h_2, is accomplished numerically. The linearity of the problem, together with the simple form of the boundary conditions, suggest the use of a superposition technique (Roberts & Shipman 1972). A collection of initial-value problems associated with (4.2) is solved numerically, each with appropriate end conditions so that any linear combination of these solutions satisfies one boundary condition. The only remaining task is to find that particular linear combination which satisfies the second boundary condition. The desired reflection coefficient R_1 is then determined algebraically once the ϕ_n and ϕ_n' are known.

5. Discussion and numerical results

The boundary-value problem is solved with selected sets of shape- and depth-function parameters in order to quantify the dependence of the reflection of the single incident mode $e^{iK_1 x} \sin \frac{1}{2}y$ on those parameters. Of principal interest is the comparison of $|R_1(K_1)|$ in the case of constant depth ($h_2 = 1$) with those $|R_1(K_1)|$ curves obtained for the same harbour shape (γ, ρ_+, ρ_-) but with variable depth incorporated via (3.9). The range of parameters for which interesting behaviour in $|R_1(K_1)|$ is anticipated can be delimited by examining $S_1(x)$ given in (4.3).

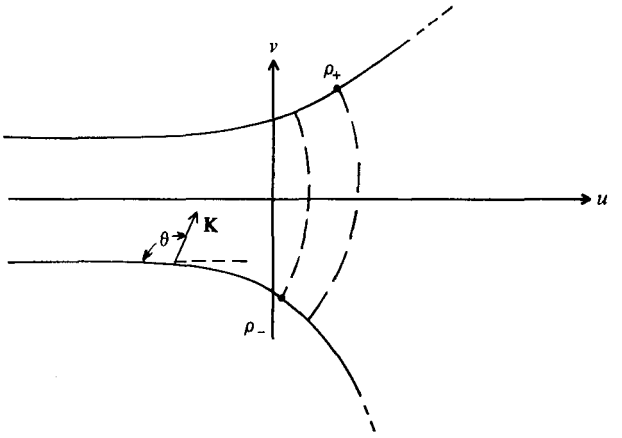

FIGURE 10

The major feature governing the reflection due to changing depth appears in (3.10), prior to the eigenfunction decomposition. From that equation it is evident that, if $h(x)$ increases more rapidly than $|f'(z)|^2$ as $x \to \infty$, then the reflected wave must have unit amplitude. In the eigenfunction description (4.2), this corresponds to a one-turning-point problem where $S_1(x < x_0) > 0$ and $S_1(x > x_0) < 0$ for some x_0, and wave trapping within the harbour is guaranteed. The numerical results have shown, however, that the less dramatic depth function with $h_2 = 2$ leads to values of $R_1(K_1)$ that are so close to 1 that, over the limited range of K_1 for which this statement is true, no new information is obtained by increasing the final depth. All of the variable-depth results recorded here were obtained using $h_2 = 2$. Furthermore, the value of SHIFT in (3.9) was chosen so that for all of the symmetric profiles in figures 5 and 6 the mean depth ($\frac{3}{2}$) is located along that curve which terminates at the point of maximum curvature on the boundary. These are shown as the dashed lines in figures 5 and 6. This choice is arbitrary, though, to a degree, it standardizes the various shapes. Loosely stated, half of the net depth variation is accomplished within the harbour, and the remaining changes take place in the region exterior to the point of maximum rate of opening, for each geometry.

Specifying h_2 and SHIFT in this way ensures that not only will the mapping function dominate as $x \to \infty$, but that a two-turning-point problem emerges with $S_1(x < x_0) > 0$, $S_1(x_0 < x < x_1) < 0$ and $S_1(x > x_1) > 0$, for some x_0 and x_1. The size of $|R_1|$ correlates with the size of $|x_1 - x_0|$. The incident wave must negotiate a region where the fundamental solutions are non-oscillatory, and its ability to transmit any energy through the region diminishes as $|x_1 - x_0|$ increases. A simple model can be used to clarify the nature of the dependence of $|R_1|$ on the remaining parameters ρ_+, ρ_-, s, γ.

The incident-wave shape at $u = -\infty$ can be viewed as a single cross-wave whose successive reflections within the parallel-wall region produces a standing wave in v ($\sin \frac{1}{2}v$) and allows for propagation in the positive u-direction ($e^{iK_1 u - i\omega t}$) (figure 10).

As the wave encroaches on the variable-depth region, the downstream side of a wavefront tends to move faster, since locally $c = (gh)^{\frac{1}{2}}$ is larger, causing the wave vector **K** to turn. If the depth profile is such that $\theta \to \frac{1}{2}\pi$ within the parallel boundary domain a standing wave is established and $|R_1|$ must equal 1. The geometries that would lead to such a result are those where $s \to 0$, so that the refractive effects of variable depth begin further to the left, and those where $\rho_+, \rho_- \to 0$, so that half of

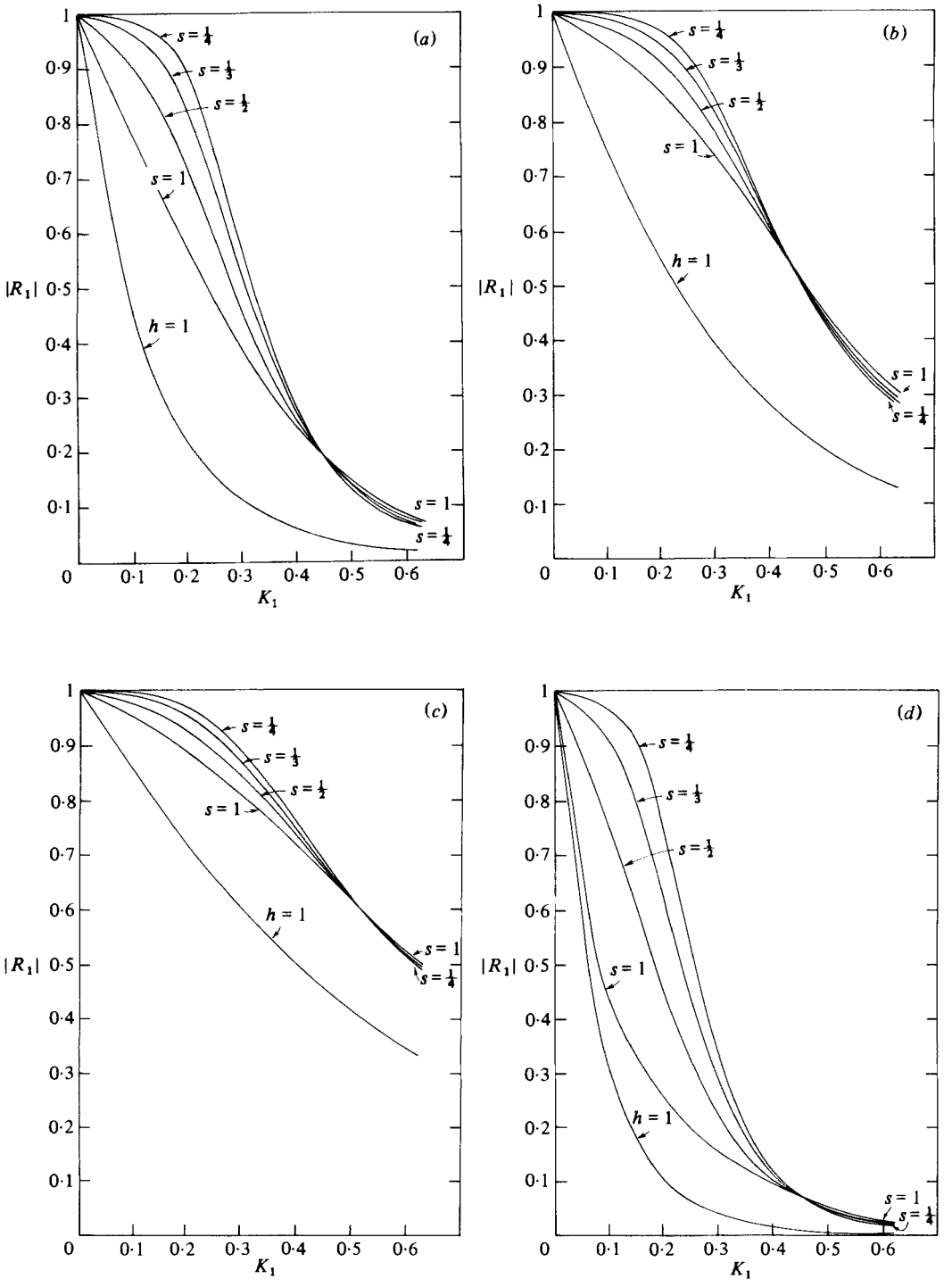

FIGURE 11 (*a–d*). Fort caption see facing page.

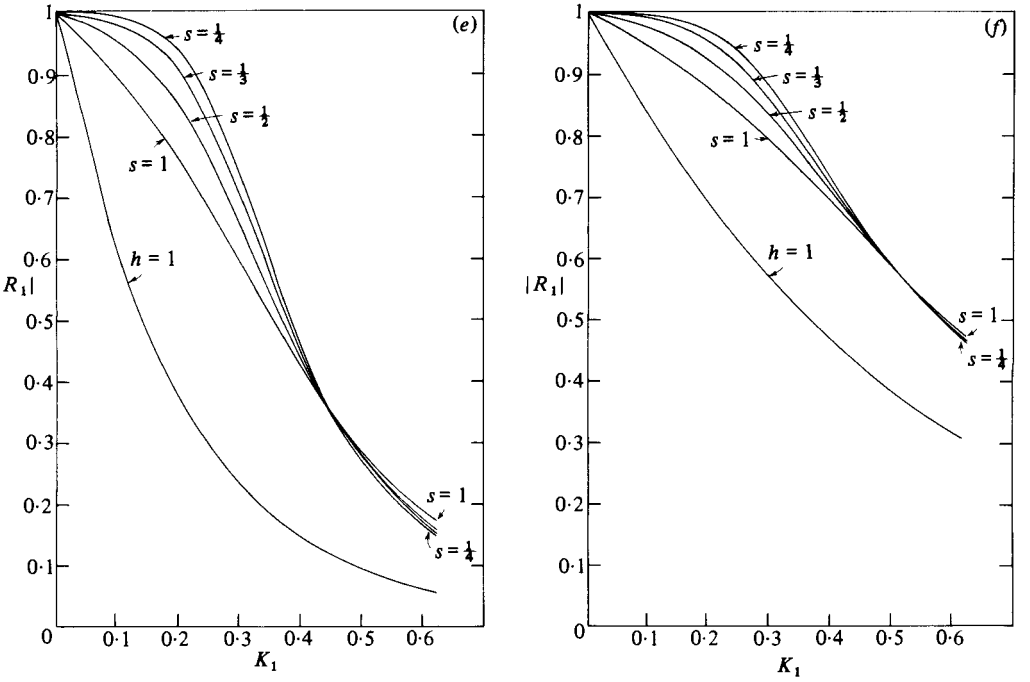

FIGURE 11. $|R_1(K_1; s)|$ for (*a*) $\gamma = 0{\cdot}6$, $\rho_{\min} \approx 2{\cdot}8$; (*b*) 0·6, 1·3; (*c*) 0·6, 0; (*d*) 0·5, 5·2; (*e*) 0·5, 2·2; (*f*) 0·5, 0.

the net depth variation is confined to the channel. If changes in $h(x)$ only begin where the harbour has started to widen substantially ($\rho_+, \rho_- \gg O(1)$, $s \geqslant O(1)$), the wall reflections can no longer produce a standing wave, and the ensuing leakage of energy reduces the value of $|R_1|$. These trends are in evidence in all of the numerical results that follow.

Primary consideration is given to symmetric profiles for which solutions are obtained by using only the odd-numbered mode equations in (4.2). The combined effects of variable width and depth can be assessed in general terms using these simpler shapes. The magnitude of the reflection coefficient R_1 is plotted as a function of K_1 in figure 11 for each of the six symmetric shapes shown in figures 5 and 6. Each graph gives $|R_1(K_1)|$ for a fixed harbour profile, where only the depth transition length s is varied. Note that, for a given opening angle $2\pi\gamma$, those graphs (figure 11*c*,*f*) corresponding to geometries where ρ and s are small invariably show the maximum $|R_1|$ values. Not surprisingly, the distance over which $S_1(x) < 0$ in the mapped plane is also greater in these cases.

Asymmetry of the harbour shape will necessarily imply both even- and odd-mode behaviour. Since no natural harbour possesses pure symmetry, the key issue is to determine the extent to which asymmetry provides a radiational leak in the nearly resonant behaviour shown to exist in some of the simpler shapes. Appealing directly to the coupled system (4.2), it is apparent that, even under those conditions that lead to $S_1(x) < 0$ in some region, the corresponding function $S_0(x)$ associated with the plane-wave mode is positive for all x. Thus a fraction of the wave energy incident from the left will be coupled into ϕ_0 during its passage through the transition zone and will continue to propagate seaward. This energy leakage will necessarily diminish the value of $|R_1|$ that would have prevailed had the harbour been symmetric with roughly the same values of $2\pi\gamma$, ρ and s. The numerical results have shown, however,

that strong leakage does not occur, and that the $|R_1|$ dependence on $2\pi\gamma$, s and the boundary curvature follows a pattern similar to that established for the symmetric-harbour results.

Plots of $|R_1|$ are presented for the profile in figure 7 in which $\alpha = 0{\cdot}8$, $\gamma = 0{\cdot}4$ and $\beta = 1$. The symmetric case that provides the most direct comparison with this example is given in figure 5 with $\alpha = \delta = 0{\cdot}6$ and $\beta = 1$. The boundary curvatures near $u = 0$ can be considered approximately equal, since $\beta = 1$ in both cases, and the net included angles at ∞ are the same. The potentially significant difference between the symmetric and asymmetric shapes being compared lies in the location of the mean depth. The consequences of this discrepancy are explored by obtaining $|R_1|$ plots for the two different locations of the mean depth shown in figure 7. The numerical results indicate, however, that just as these two positions straddle the location of the mid-depth contour in the corresponding symmetric harbour, the $|R_1|$ curves presented in figure 12 for the asymmetric harbour straddle the curves shown in figure 11 (*a*), where $\alpha = \delta = 0{\cdot}6$. An obvious correspondence between the symmetric and asymmetric harbours suggested by this result was found to prevail in all the numerical experiments with asymmetric shapes. The $|R_1|$ values when $\rho_+ \neq \rho_-$ will be very nearly the same as those generated by a symmetric shape with the same γ and s values, and an averaged position of the mean depth. Thus the behaviour of the first odd mode at $u = -\infty$ in an asymmetric profile can be regarded as nearly equal to the total wave field at $u = -\infty$ in an 'equivalent' symmetric harbour.

The substantial increase in $|R_1|$ found in both symmetric and asymmetric profiles (a doubling was not uncommon) due to the inclusion of seemingly benign variations in the local depth, indicates that it cannot be simply an artifact of the highly idealized nature of the shapes. The details of the wave behaviour in a real harbour would, of course, never be duplicated by this analysis. Yet, for an open harbour whose most macroscopic features near the bay entrance can be described by $f(z)$, the strong reflections shown to prevail using the idealized shapes could be a prominent component of the overall behaviour of such a harbour. One important manifestation of an increase in $|R_1|$ is outlined next, where the results for an infinite channel are used to forecast the durability of the wave motion in a harbour of finite extent.

The total wave field at a distance far to the left of the origin is given approximately by

$$\phi_{\text{tot}} \approx (e^{iK_1 u} + R_1 e^{-iK_1 u}) \sin \tfrac{1}{2}v\, e^{-i\omega t} + O(e^{|K_3|u}). \tag{5.1}$$

This expression is strictly valid for symmetric shapes only, though it can be used for asymmetric harbours using the correspondence rule cited above. A more convenient form of (5.1) for the present purpose is

$$\phi_{\text{tot}} = 2R^{\frac{1}{2}} \sin \tfrac{1}{2}v\, e^{-i\omega t} \cos (K_1 u + \tfrac{1}{2}i \ln R), \tag{5.2}$$

where $|R| = R_1 e^{i\psi}$ and $-\pi \leqslant \psi \leqslant \pi$. A rigid wall placed at a value of u where (5.2) is appropriate disrupts the steady-state behaviour implicit in that equation, and the attendant boundary condition induces a complex-valued K_1. The requirement

$$\left.\frac{\partial \phi_{\text{tot}}}{\partial u}\right|_{u=-L} = 0$$

implies that

$$K_1 = \frac{i \ln R}{2L} + \frac{n\pi}{L},$$

provided that L is large enough that the final term in (5.1) can be ignored. The choice $n = 0$ corresponds to the lowest mode shape in u, and the resulting wave motion near

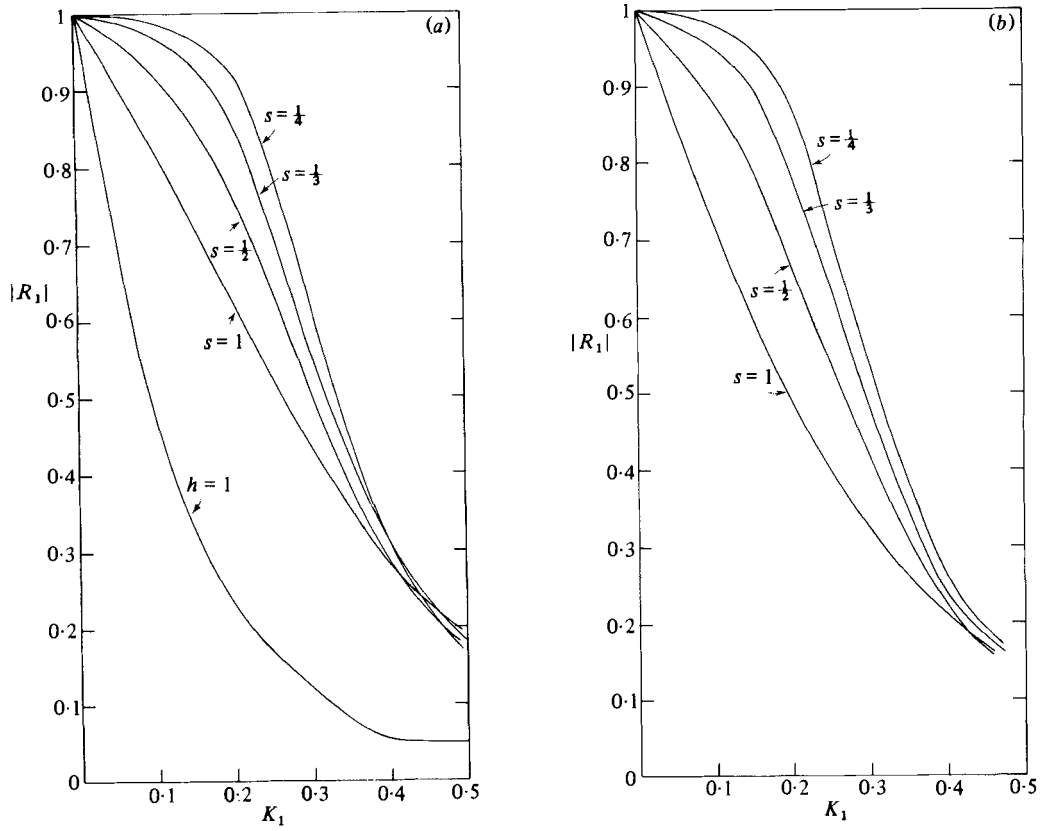

FIGURE 12. $|R_1(K_1;s)|$ when $\alpha = 0{\cdot}8$, $\delta = 0{\cdot}4$, $\beta = 1$, and SHIFT $\approx -0{\cdot}8$ (*a*) and 0 (*b*).

the wall is described by

$$\phi_{\text{tot}} = 2R^{\frac{1}{2}} \sin \tfrac{1}{2}v\, e^{-i\omega t}\left[\cosh \frac{\ln |R|}{2L} \cos \frac{\psi}{2L}(u+L) + i \sinh \frac{\ln |R|}{2L}(u+L) \sin \frac{\psi}{2L}(u+L)\right]. \quad (5.3)$$

Although (5.3) is an appropriate description only in the harbour's innermost region, it can be used for a qualitative assessment of the reflection process throughout the harbour. The small value of $\psi/2L$ implies a very long wave, whose shape near $u = -L$ coincides with that of a wave completing a half-cycle in a distance $2L\pi/\psi$. In the nearly resonant cases, the phase was found to approach π as $|R_1| \to 1$. Thus the 'effective length' of the harbour is $2L$ when $|R_1| \to 1$, and, consistent with total reflection, a standing wave in u emerges. When less than total reflection prevails in the infinite-harbour geometry, the wave amplitude in the finite domain decays owing to the complex-valued frequency. The frequency ω and the wavenumber $K_1 = i \ln R/2L$ are related by

$$\frac{\omega b}{(gh_0)^{\frac{1}{2}}} = K_0 = \tfrac{1}{2}(1 + (2K_1)^2)^{\frac{1}{2}},$$

implying the following approximate formulas for the real and imaginary parts of ω,

valid when $|\ln R|/L \ll 1$:

$$\mathrm{Re}\,(\omega) = \frac{(gh_0)^{\frac{1}{2}}}{2b}\left(1+\frac{\psi^2-\ln^2|R|}{2L^2}\right), \quad \mathrm{Im}\,(\omega) = \frac{(gh_0)^{\frac{1}{2}}}{2bL^2}\,|\psi|\,\ln|R|.$$

The damping factor, when written using the dimensional lengths of figure 1, is then

$$\exp\left[\frac{t}{T_0}\frac{2b\pi}{2\tilde{L}}\,|\psi|\,\ln|R|\right], \tag{5.4}$$

where $T_0 = 2\pi\tilde{L}/(gh_0)^{\frac{1}{2}}$ is the period of the natural mode of oscillation in the $\tilde{x}$-direction. Equation (5.4) exhibits the dependence of the e-folding time on R, which, to cite a mild example, is increased by roughly a factor of 6 as $|R|$ increases from 0·5 to 0·9.

6. Conclusions

It has been established that there are geometries (planforms and depth variations) for which, in the non-dissipative approximation, the wave energy in selected modes will not leak out at all. Furthermore, the results indicate that, for more realistic geometries ($h_2 \neq \infty$), mild variations in the depth can still provide a very effective trapping mechanism that dramatically increases the e-folding times of some modes. It therefore seems reasonable to conclude that in real open-bay geometries the balance between the deepening and the planform geometry exploited in the foregoing analysis could be a substantial contribution to the long decay times that are sometimes observed in such harbours.

Some of the work reported here was included in a doctoral thesis submitted to Harvard University in June 1980. The author is deeply grateful for the continued guidance provided by his thesis advisor, Professor George F. Carrier. The advice and help of Professor J. L. Sanders and Professor D. G. M. Anderson is also gratefully acknowledged. Funding for this research was provided by the National Science Foundation under Grants MCS78-07598 and PFR79-21774.

Appendix. Properties of the mapping function

In this appendix the formulas used to describe the harbour profiles in the dimensionless physical plane are derived. Relating the mapped plane $x+iy$ to the physical plane $u+iv$ requires a numerical procedure, since

$$f'(z) = (1+\exp\,(\tfrac{1}{2}i\pi(\alpha-\delta))\,e^{\frac{1}{2}(\alpha+\delta)z})^{\beta}$$

is not integrable in closed form. An expression for the curvature of either the top or bottom boundary can be derived immediately, however, as it involves only derivatives of f. The curvature K is given by

$$K = \frac{1}{|f'(z)|}\,\mathrm{Im}\left(\frac{f''(z)}{f'(z)}\right),$$

and the value of x that results in the minimum radius of curvature of the top (bottom) boundary is found by solving for x in the equation $dK/dx = 0$ when $y = \pi$ ($y = -\pi$).

The $u+iv$ and $x+iy$ variables are formally related by the expression

$$u(x,y)+iv(x,y) = \lim_{S_0\to\infty}\left[\int_T f'(x)\,dz - S_0\right], \tag{A 1}$$

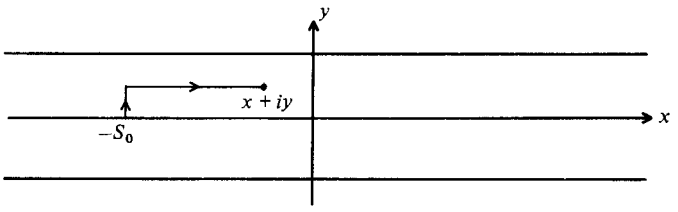

FIGURE 13

where the contour T is taken to be as in figure 13, terminating at the desired point $x+iy$. The vertical segment of T yields a contribution iy, so that (A 1) can be written as a real integral:

$$u(x,y)+i(v(x,y)-y) = \lim_{S_0\to\infty}\left[\int_{-S_0}^{x}(1+\exp(\tfrac{1}{2}i\pi(\alpha-\delta))\,e^{\frac{1}{2}(\alpha+\delta)(t+iy)})^{\beta}\,dt-S_0\right].$$

The term $1+\exp\frac{1}{2}i\pi(\alpha-\delta))\,e^{\frac{1}{2}(\alpha+\delta)(t+iy)}$ may be written as $\tau+i\mu$ and cast as an exponential, thereby separating the real and imaginary parts of the integrand. The variables u and v are then related (albeit in a cumbersome manner) to the resulting real integrals in x and y.

REFERENCES

IPPEN, A. T. (ed.) 1966 *Estuary and Coastline Hydrodynamics*. McGraw-Hill.

KAJIURA, K. 1961 On the partial reflection of water waves passing over a bottom of variable depth. *IUGG Monograph* no. 24.

KRAUTCHENKO, J. & MCNOWN, J. S. 1955 Seiche in rectangular ports. *Q. Appl. Math.* **13**, 19–26.

LAUTENBACHER, C. C. 1970 Gravity wave refraction by islands. *J. Fluid Mech.* **41**, 655–672.

LEE, J. J. 1971 Wave-induced oscillations in harbours of arbitrary geometry. *J. Fluid Mech.* **45**, 375–394.

ROBERTS, S. M. & SHIPMAN, J. S. 1972 *Two-Point Boundary Value Problems; Shooting Methods*. Elsevier.

ROSEAU, M. 1952 Contribution à la théorie des ondes liquides de gravité en profondeur variable. *Publ. Sci. et Tech. du Ministère de l'Air* no. 275, Paris.

SHEN, M. C., MEYER, R. E. & KELLER, J. B. 1968 Spectra of water waves in channels and around islands. *Phys. Fluids* **11**, 2289–2304.

STOKER, J. J. 1957 *Water Waves*. Interscience.